

UKPGAN: Unsupervised KeyPoint GANeration

Yang You, Wenhai Liu, Yong-Lu Li, Weiming Wang, Cewu Lu*

Shanghai Jiao Tong University, China

{qq456cvb, sjtu-wenhai, yonglu_li, wangweiming, lucewu}@sjtu.edu.cn

Abstract

Keypoint detection is an essential component for the object registration and alignment. However, previous works mainly focused on how to register keypoints under arbitrary rigid transformations. Differently, in this work, we reckon keypoints under an information compression scheme to represent the whole object. Based on this, we propose UKPGAN, an **unsupervised** 3D keypoint detector where keypoints are detected so that they could reconstruct the original object shape. Two modules: **GAN-based keypoint sparsity control** and **salient information distillation** modules are proposed to locate those important keypoints. Extensive experiments show that our keypoints preserve the semantic information of objects and align well with human annotated part and keypoint labels. Furthermore, we show that UKPGAN can be applied to either rigid objects or non-rigid SMPL human bodies under arbitrary pose deformations. As a keypoint detector, our model is stable under both rigid and non-rigid transformations, with local reference frame estimation. Our code is available on [github](#).

1. Introduction

Recently, 3D object analysis and scene understanding receive more and more attentions. Though plenty of methods [6, 17, 22, 12] on object analysis have been proposed, there is still a lack of capability of processing and understanding objects, especially under an unsupervised setting.

3D keypoints, unlike part annotations, provide a sparse but meaningful representations of an object. They are widely leveraged in many tasks such as object matching, object tracking, shape retrieval and registration [21, 4, 31]. Keypoint detections have its origin in 2D image processing [25, 20, 11]. In 3D domain, traditional methods like Harris-3D [26], HKS [27], Salient Points [5], Mesh Saliency [16], ISS [37], Sift-3D [20] and Scale Dependent Corners [23] propose to detect keypoints based on geometric variations. However, these hand-crafted detectors rely heav-

ily on hard-coded parameters and do not capture semantic information.

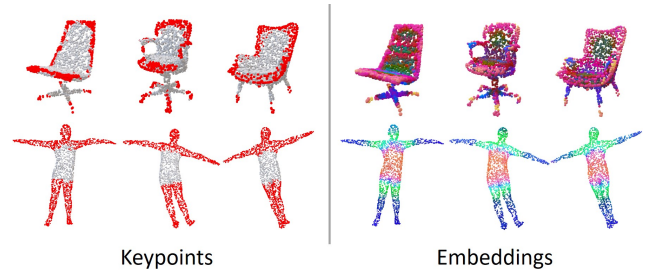


Figure 1: Our model outputs keypoints and embeddings unsupervisedly given a point cloud, in either rigid or non-rigid deformations. Left are keypoint predictions (indicated by red) and right are embedding predictions, best viewed in color. These keypoints and embeddings are *consistent* within each class.

Recently, some deep learning methods like USIP [18] and D3Feat [2] on unsupervised keypoint detection have been proposed. USIP regresses keypoint locations from pre-segmented local groups and then utilizes a probabilistic chamfer loss. However, their method requires hard-coded farthest point sampling and may output points that are not on the input. D3Feat instead gives saliency scores and descriptors densely for each point. Both USIP and D3Feat predict 3D keypoints unsupervised by solving the auxiliary task of correctly estimating rotations in a siamese architecture. They actually answer the question of *what points are stable under arbitrary rotations for an object*, while what is more interesting is that *what is the minimum set of keypoints that qualify important information of the original object*. Can we achieve both, having an informative keypoint detector that is stable under arbitrary rigid/non-rigid transformations?

To answer this question, we follow a totally different route to obtain 3D keypoints, which is named **Unsupervised Key Point GANeration (UKPGAN)**. A keypoint saliency distribution is given through a detector network, with a novel adversarial **GAN loss to control its sparsity**. Then, to make these keypoints informative, we leverage a **salient informa-**

*Cewu Lu is the corresponding author.

tion distillation process to reconstruct the original point cloud from these sparse keypoints, forming an encoder-decoder architecture. Our model can be seen as an *information compression scheme*, keeping most information of the object with the least keypoints. The rationale behind our method is simple but powerful: one should be able to fully recover an object’s structure from a small set of keypoints. This also coincides with that is mentioned in [32]: “*much of human learning, perception, and cognition, may be understood as information compression*”. Results show that our model could output stable informative keypoints from unseen objects, together with their high-dimensional embeddings without any supervision (Figure 1).

Compared to previous methods, UKPGAN has the following advantages: 1) our detector are proven to be rotation invariant without any data augmentations, by first estimating a Local Reference Frame (LRF), which also makes our local keypoint representation disentangled from rotations; 2) detected keypoints are intra-class consistent and stable on both rigid and non-rigid objects; 3) our method delivers rotation invariant feature embeddings in an unsupervised way, which are intra-class consistent.

We evaluate our method on ShapeNet models with both part labels and keypoint labels. Our model achieves remarkable results in keep consistent with human labeled part and keypoints. We further show that UKPGAN is rotation invariant by achieving high rotation repeatability. Finally, we demonstrate that our model cannot only be applied to rigid but non-rigid objects by evaluating consistency on SMPL human body deformable meshes.

2. Related Work

2.1. Hand-crafted Keypoint Detectors

Prior to the emerge of deep learning, researchers proposed numerous methods to detect stable interest points on objects, in both 2D and 3D domains. SIFT [20], ORB [25] and SURF [3] extract features by detecting local pattern variations on 2D images. They are robust to scale and rotation changes and give consistent keypoints on two identity objects. 3D Harris [26] extends Harris corner detector to 3D meshes. HKS [27] proposes a novel point signature based on the properties of the heat diffusion process on a shape. Salient Points [5] model interest points by a Hidden Markov Model (HMM), which is trained in an unsupervised way by using contextual 3D neighborhood information. Mesh Saliency [16] defines mesh saliency in a scale-dependent manner using a center-surround operator on Gaussian-weighted mean curvatures. CGF [14] learns to represent the local geometry around a point in an unstructured point cloud. 3D SIFT [20] is an analogue of the scale-invariant feature transform (SIFT) for three-dimensional images. ISS [37] introduces intrinsic shape signature, which

uses a view-independent representation of the 3D shape to match shape patches from different views directly. However, these methods only consider the local geometric information without semantic knowledge, leading a discrepancy from human perceptions.

2.2. Learning-based Keypoint Detectors

Recently, some deep learning based detectors have been proposed to bypass hand-crafted keypoint detection rules, in both 2D and 3D domains. On 2D images, some unsupervised keypoint detection methods are proposed. Jakab et al. [13] extracts semantically meaningful keypoints by passing a target image through a tight bottleneck to distill the geometry of the object. Zhang et al. [36] uses an auto-encoding module with channel-wise softmax operation to discover landmarks. Suwajanakorn et al. [29] discover latent 3D keypoints from 2D images by enforcing multi-view consistency. Georgakis et al. [8] employ a Siamese architecture augmented by a sampling layer and a novel score loss function to detect keypoints on depth maps. In 3D domain, methods like SyncSpecCNN [34] and deep functional dictionaries [28] rely under ground-truth keypoint supervision. For unsupervised methods, USIP [18] regresses keypoint locations from pre-segmented local groups and then utilizes a probabilistic Chamfer loss. D3Feat [2] instead gives saliency scores and descriptors densely for each point. It relies on an auxiliary task of correctly estimating rotations in a siamese architecture, ignoring semantic information. A similar work [7] tries to learn category-specific symmetric 3D keypoints but it still resort to farthest point sampling and groups keypoints in Euclidean space, making these keypoints agnostic to the global information of the entire object.

3. Approach

3.1. Overview

Given a point set $\mathbf{X} = \{\mathbf{x}_n | \mathbf{x}_n \in \mathbb{R}^3, n = 1, 2, \dots, N\}$ with \mathbf{x} sampled from some manifold \mathcal{M} , we seek a keypoint set $\tilde{\mathbf{X}} \subseteq \mathbf{X}$, where $|\tilde{\mathbf{X}}|$ is the number of required keypoints.

Here, we propose an unsupervised encoder-decoder architecture. In the encoder, which is also the detector, a keypoint probability s is predicted for each point. To keep the detected keypoints sparse, GAN-based keypoint sparsity control is leveraged. In the decoder, also a reconstruction network, we utilize salient information distillation to reconstruct the original point cloud, in an unsupervised way. The intuition is that, a set of good keypoints should contribute to the unique information of an object, making reconstruction possible. The overview of our method is shown in Figure 2.

3.2. Rotational Invariant Feature Extraction

In order to be robust under rigid transformations, we first generate a Local Reference Frame (LRF) by covariance

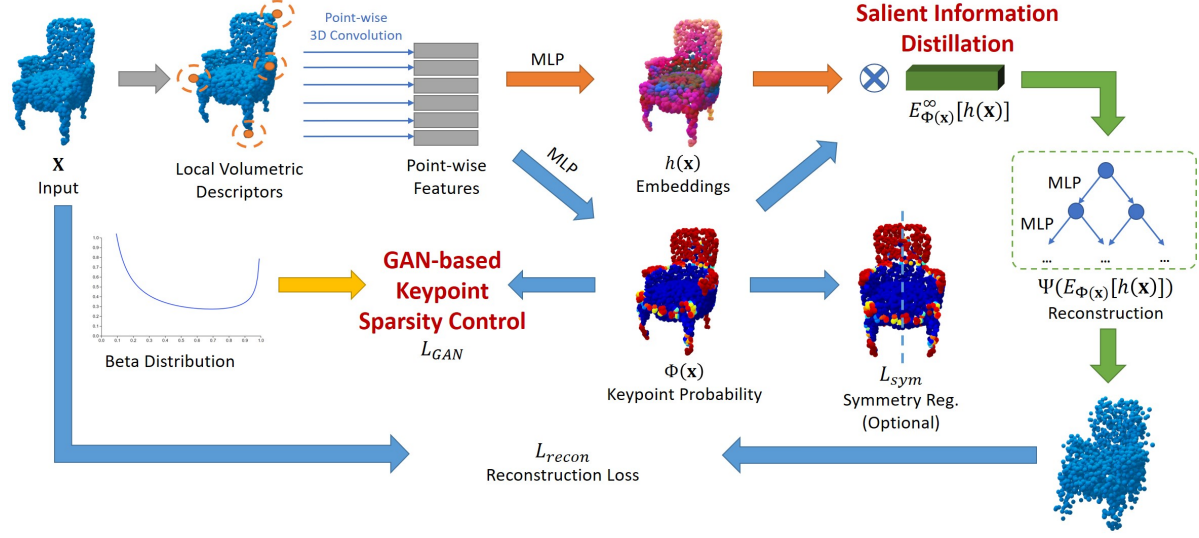


Figure 2: **Our whole pipeline on keypoint and embedding generations.** We first extract point-wise rotation invariant features and then output keypoint probabilities and semantic embeddings through two MLPs, respectively. GAN is leveraged to control keypoint sparsity and salient information distillation is utilized to distill most salient features. A decoder is concatenated to reconstruct original point clouds.

eigen-decomposition on each point \mathbf{x} 's spherical neighborhoods $\mathcal{S} = \{\mathbf{x}_i : \|\mathbf{x}_i - \mathbf{x}\|_2 \leq r\}$. Then points in the local neighborhood $\mathbf{x}_i \in \mathcal{S}$ are transformed to their canonical position \mathbf{x}'_i according to the estimated LRFs. Next, we follow the same strategy as that in PerfectMatch [9] to discretize these points in a Smoothed Density Value (SDV) grid, centered on the point \mathbf{x} and aligned with the LRF. The voxelization is based on Gaussian smoothing kernel. Afterwards, we would get a voxelized descriptor $\mathcal{F}(\mathbf{x}) \in \mathbb{R}^{W \times H \times D}$ for each point \mathbf{x} . For mode details, we refer the reader to PerfectMatch [9]. These point-wise 3D descriptors are batched together and fed through 3D convolution layers to be further refined. Thanks to the estimated LRFs, this step provides *local rotation-invariant* features, which are critical for rotation repeatability.

3.3. Dual Branches on Estimating Probabilities and Embeddings

After extracting rotation invariant point-wise features, we use dual Multi-Layer Perceptron (MLP) networks to estimate a keypoint salient probability $\Phi(\mathbf{x}) \in [0, 1]$ and a high-dimensional embedding $h(\mathbf{x}) \in \mathbb{R}^F$, which will be used for reconstruction. The two parameters α and β controls the accumulation of positive (1) and negative (0) samples.

Sparsity on $\Phi(\mathbf{x})$. In order to compress the entire point cloud with a minimum set of keypoints, $\Phi(\mathbf{x})$ needs to be sparse. What is a good way to make $\Phi(\mathbf{x})$ sparse? One would consider L1 regularization. However, it tends to out-

put more probabilities around zero and does not have much control over non-zero probabilities. In order to output distinguishable keypoints, we would like $\Phi(\mathbf{x})$ to accumulate around both 0's and 1's. Therefore, Beta distribution (shown in Figure 2) is leveraged and we would like our keypoint distribution to match it.

GAN-based Keypoint Sparsity Control Since we are estimating keypoint distribution *samples* instead of distribution *parameters*, a closed form of KL divergence between Beta prior and $\Phi(\mathbf{x})$ does not exist. We resort to adversarial loss. GAN [10] is leveraged to force a prior Beta distribution on the keypoint probability $\Phi(\mathbf{x})$. The model assumes that an additional neural network: discriminator D , which is responsible for distinguishing between fake and true samples, where the true samples are sampled from assumed prior Beta distribution $p(\cdot)$ and fake samples are generated via saliency estimation network $\Phi(\cdot)$.

In our experiments, we employ WGAN-GP [1] instead of the naive GAN loss as it is more robust. The loss follows:

$$L_{GAN} = \min_{\Phi} \max_D [\mathbb{E}_{\mathbf{x} \sim p} [D(\mathbf{x})] - \mathbb{E}_{\mathbf{x} \sim \mathcal{M}} [D(\Phi(\mathbf{x}))]] \quad (1)$$

$$+ \lambda (\|\nabla_{\mathbf{x}} D\|_2 - 1)^2, \quad (2)$$

which penalizes the gradient of the discriminator.

3.4. Reconstruction Network

Given a keypoint distribution $\Phi(\mathbf{x}) \in \mathbb{R}$ and high-dimensional embeddings $h(\mathbf{x}) \in \mathbb{R}^F$, we now introduce an

unsupervised reconstruction loss with the keypoint-expected feature. Denote the point cloud decoder as $\Psi : \mathbb{R}^F \rightarrow \mathbb{R}^{N \times 3}$, the reconstruction loss can be expressed as follows:

$$L_{recon} = \text{ChamferDistance}(\Psi(\mathbb{E}_{\Phi(\mathbf{x})}[h(\mathbf{x})]), \mathbf{X}),$$

$$\mathbb{E}_{\mathbf{x} \sim \Phi(\mathbf{x})}[h(\mathbf{x})] = \sum_{\mathbf{x} \sim \mathcal{M}} \frac{\Phi(\mathbf{x})}{Z(\Phi)} \cdot h(\mathbf{x}), \quad (3)$$

where $Z(\Phi) = \sum_{\mathbf{x} \sim \mathcal{M}} \Phi(\mathbf{x})$.

In our implementation, the point cloud decoder Ψ has a similar structure with that in TopNet [30] and $h(\mathbf{x})$ is L2-normalized.

Salient Information Distillation In order to distill out salient keypoint information, we incorporate a heat temperature parameter γ . Equation 3 becomes:

$$\mathbb{E}_{\Phi(\mathbf{x})}^\gamma[h(\mathbf{x})] = \sum_{\mathbf{x} \sim \mathcal{M}} \frac{\Phi(\mathbf{x})^\gamma}{Z(\Phi, h)} \cdot h(\mathbf{x})^\gamma. \quad (4)$$

When $\gamma = 1$, Equation 4 equals Equation 3; when $\gamma = \infty$, the most salient keypoint information is distilled out and Equation 4 becomes,

$$\mathbb{E}_{\Phi(\mathbf{x})}^\infty[h(\mathbf{x})] = \max_{\mathbf{x} \sim \mathcal{M}} [\Phi(\mathbf{x}) \cdot h(\mathbf{x})]. \quad (5)$$

In addition, we care about the absolute value of $h(\mathbf{x})$ (features with large negative magnitude should not be suppressed) and the final equation is

$$\mathbb{E}_{\Phi(\mathbf{x})}^\infty[h(\mathbf{x})] = \max_{\mathbf{x} \sim \mathcal{M}} [\Phi(\mathbf{x}) \cdot \max(h(\mathbf{x}), 0)] \quad (6)$$

$$\oplus \max_{\mathbf{x} \sim \mathcal{M}} [\Phi(\mathbf{x}) \cdot \max(-h(\mathbf{x}), 0)], \quad (7)$$

where \oplus means concatenation.

Indistinguishable points are therefore discarded rather than summed over. These points are useless and should have little contribution to the final reconstruction. For example, a rectangle can be perfectly reconstructed given the four corners. Points between the corners provide little information about the overall shape. Detailed analysis on salient information distillation will be given in Section 4.4.

3.5. Symmetric Regularization

Although we first extract rotation invariant local descriptors from original point clouds, it is not symmetric invariant. For most common objects, we have a strong prior such that detected keypoints and features should be symmetric, leading to the following loss:

$$L_{sym} = \frac{1}{|\mathbf{S}|} \sum_{(\mathbf{x}, \mathbf{x}') \in \mathbf{S}} (\|\Phi(\mathbf{x}) - \Phi(\mathbf{x}')\| + \|h(\mathbf{x}) - h(\mathbf{x}')\|_1), \quad (8)$$

where \mathbf{S} is the set of all symmetric point pairs. Note that symmetric regularization is only used for training; in testing, symmetric information about objects is not required.

The final loss is an empirical sum of three terms:

$$L = \beta_1 \cdot L_{recon} + \beta_2 \cdot L_{GAN} + \beta_3 \cdot L_{sym}. \quad (9)$$

3.6. Implementation Details

Network Architecture Our model takes a point cloud $\mathbf{X} \in \mathbb{R}^{N \times 3}$ as input where $N = 2048$. Then a voxelized descriptor is extracted for each point with $\{\mathcal{F}(\mathbf{x}_n)\}_{n=1}^N \in \mathbb{R}^{N \times W \times H \times D}$. Then these descriptors are fed into seven 3D convolution layers with channels 32, 32, 64, 64, 128, 128, 128. To predict $\Phi(\mathbf{x})$, three-layer MLP with channels 512, 256, 1 is employed; for $h(\mathbf{x})$, three-layer MLP with channels 512, 256, 128 is employed and the embedding dimension is 128. These two branches share the first two layers.

For WGAN-GP network, we use five *conv1d* layers (with channels 512, 256, 128, 64, 1) and a *max-pooling* layer for the critic function D . The gradient penalty coefficient $\lambda = 1$.

For the decoder, we leverage a similar structure with TopNet [30]. Specifically, the decoder has 6 levels and each MLP in the decoder tree generates a small node feature embedding of size 8. When generating $N = 2048$ points, the root node has 4 children and all other internal nodes in subsequent level generate 8 children. Each MLP in the decoder is a has 3 stages with 256, 64, and 8 channels respectively.

Hyperparameters and Training For ShapeNet models, we choose $\beta_1 = 10.$, $\beta_2 = 1$, $\beta_3 = 0.1$ through the validation set; for SMPL human body dataset, we choose $\beta_1 = 10.$, $\beta_2 = 1$, $\beta_3 = 0$. In all our experiments without specification, the beta prior distribution is fixed with $\alpha = 0.01$ and $\beta = 0.05$. The parameters of the network are optimized using ADAM [15], with learning rate $1e-4$.

4. Experiments

In experiments, we evaluate our method on both rigid and non-rigid datasets to show its capability on detecting stable interest points on general objects. We first conduct experiments on ShapeNet part models to show the intra-class consistency between the keypoints. Then we compare these keypoints with human annotated ones. Next, keypoint repeatability under arbitrary rotations is evaluated. Ablation study follows to validate our proposed components. Finally, we show that UKPGAN can be used to track stable interest points on non-rigid human bodies under different poses from SMPL models [19].

4.1. ShapeNet Part Correspondence

In this section, we measure the ability of the model to find keypoints that are consistent with model part definitions on different instances of a given category.

Dataset ShapeNet part dataset [33] is leveraged. It creates detailed per-point labeling of 31963 models in 16 shape categories in ShapeNetCore. Official training and test and split is used. Here, we evaluate on three common classes: airplane, chair and table. More results on other classes can be found in supplementary.

Metric For all detected keypoints on models, we cluster them into 8 classes with K-means. In each cluster, the ratio of keypoints that have the same part label is considered as the correspondence ratio. Mean correspondence ratio (%) is reported as the average correspondence ratio of all clusters.

Compared Algorithms We evaluate the performance of our method and compare it with five interest point detection algorithms, named USIP [18], D3Feat [2], Harris-3D [26], ISS [37] and SIFT-3D [20]. The former two algorithms are data-driven while the latter three leverage hand-crafted 3D local geometric patterns. For all methods that need training, training is done independently for each category. UKPGAN, USIP and D3Feat output keypoint probabilities which are refined through Non-Maximum-Suppression (NMS) with radius 0.1. Of the generated keypoints, 8 most salient keypoints are chosen for evaluation. The hyper-parameters of Harris-3D, ISS and SIFT-3D are the same as those in [2].

Evaluation and Results Quantitative results are shown in Table 1. We see that our model achieves higher correspondence ratio with human annotated part labels.

K-means clustering results are given in Figure 3. Our model gives a more neat clustering result on interest points. For chairs, four legs are better clustered in our model, while other methods fail to find such correspondences.

	airplane	chair	table
USIP	77.0	70.2	81.5
D3Feat	79.9	84.0	79.1
HARRIS-3D	76.9	70.3	84.2
ISS	72.2	68.1	83.3
SIFT-3D	73.5	70.9	84.1
Ours	82.8	87.4	86.4

Table 1: **Mean correspondence ratio (%) evaluated on ShapeNet part dataset.**

4.2. Comparison with Human Annotated Keypoints

In this section, we compare detected keypoints with those human annotated ones, in order to see if there is any semantic correspondence among keypoints.

Dataset Two datasets are utilized: ShapeNet-chair keypoint and KeypointNet [35] dataset. ShapeNet-chair keypoint set is proposed by SyncSpecCNN [34], which consists of thousands of keypoints annotated on ShapeNet chairs by experts. KeypointNet annotates millions of keypoints on models from 16 object categories of ShapeNet. We evaluate on airplanes, chairs and tables for KeypointNet and on chairs for ShapeNet-chair keypoint dataset. For both datasets, we randomly split them into 75%, 10% and 15% for train, val and test.

Metric We evaluate the performance by mean Intersection over Union (mIoU). Intersection is counted if the geodesic distance of a detected keypoint to its closest ground-truth is less than some geodesic threshold. Union is simply the union of detected and ground-truth keypoints.

Compared Algorithms We compare UKPGAN with USIP, D3Feat, Harris-3D, ISS and SIFT-3D. Training is done independently for each category. UKPGAN, USIP and D3Feat output keypoint probabilities which are refined through Non-Maximum-Suppression (NMS) with radius 0.1 and thresholding ($p = 0.5$).

Evaluation and Results Quantitative results are given in Figure 5. We see that UKPGAN aligns better with human annotated keypoints. It achieves much higher IoU than other methods. Qualitative visualizations are shown in Figure 4. It can be seen that UKPGAN gives keypoints that are intra-class consistent and edge/corner salient. On the contrary, both USIP and D3Feat have a “grid” artifact, especially for chair seats and desktops. Their keypoints are uniformly distributed across the entire object. For traditional keypoint detectors like Harris, ISS and SIFT, their keypoints are quite unstable and are not consistent within the same class.

4.3. Repeatability under Arbitrary Rotations

A good keypoint detector should be invariant to rotations since orientations of point clouds are often unknown. Therefore, rotation repeatability is an important metric to measure the quality of a keypoint detector.

Dataset We evaluate on the test split of KeypointNet dataset, averaged over airplane, chair and table categories.

Metric We follow the relative repeatability metric proposed in USIP as the evaluation metric. Given two point clouds of the same object, a keypoint in the first point cloud is considered repeatable if its distance to the nearest keypoint in the second point cloud is less than 0.1, under ground-truth transformations. We report the percentage of repeatable keypoints when different number of keypoints are detected.

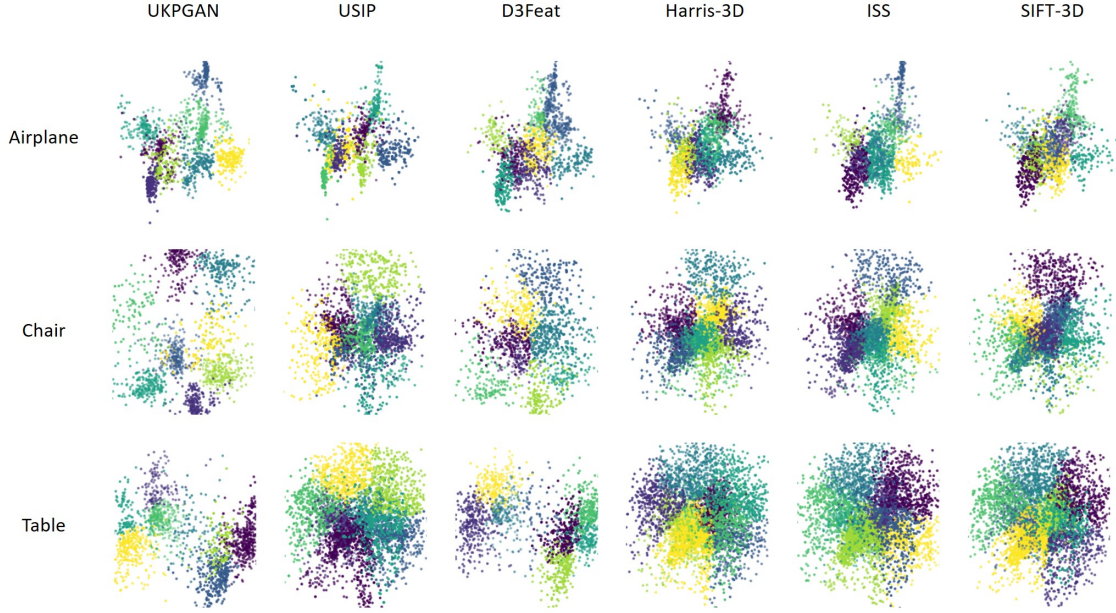


Figure 3: **Keypoint clustering results across intra-category models.** Different colors indicate different clusters. Notice that our model better clusters interest points into different parts (e.g. four legs of chairs), which is also more consistent with human labeled part annotations.

Compared Algorithms We compare UKPGAN with USIP, D3Feat, Harris-3D, ISS and SIFT-3D. Training settings follow Section 4.2. For each detector, we generate 4, 8, 16, 32, 64, 128, 256, 512 most salient keypoints by their scores and calculate the relative repeatability respectively.

Evaluation and Results The relative repeatability under arbitrary rotations for KeypointNet is shown in Figure 6. Thanks to the local reference frame (LRF) extracted in our method, we achieve much higher keypoint repeatability than all previous methods. Even when there are only four keypoints detected, we achieve nearly 100% repeatability, making UKPGAN extremely stable.

4.4. Ablation Study

In this section, we validate our design choices by conducting several ablation studies. Evaluation results are done on KeypointNet test split. Both IoU calculated with human annotations and rotation repeatability are evaluated. IoU is reported by NMS under threshold 0.1 and rotation repeatability is reported with 4 most salient keypoints under threshold 0.1. Quantitative results are listed in Table 2 and qualitative results are shown in Figure 7.

GAN-based Keypoint Sparsity Control. GAN-based Keypoint Sparsity Control is important to accumulate keypoint probabilities around both 0 and 1. We now replace it with L1 loss to form a baseline. From Figure 7, we can

see that L1 loss simply output tons of probabilities around 0, without detecting any salient keypoints. Without GAN-based sparsity control, information carried by keypoints gets lost with lower IoUs. Notice since L1 baseline gives pretty low probabilities, we threshold the probabilities with half of the maximum, to make it comparable to our complete model.

Salient Information Distillation. Salient information Distillation is another important module for our model. We compare our complete model with a baseline that implements Equation 3. It is shown that with no salient information distillation, those salient parts of models are not detected and keypoints fail to align with human annotated ones.

Local Rotational Invariant Descriptors. Local rotation invariant descriptors play an important role in maintaining repeatability under arbitrary rotations. If we replace detector module with raw XYZ features that are further processed by PointNet without rotation invariance guarantee, both keypoint IoU and rotation repeatability drop.

Symmetric Regularization. In Section 3.5, we integrate a symmetric invariance prior into our model, which is helpful since the extracted descriptors are only rotation invariant rather than symmetric invariant. If we remove symmetric regularization, we see that detected keypoints are not symmetric anymore in Figure 7, with a drop in both IoU and rotation repeatability.

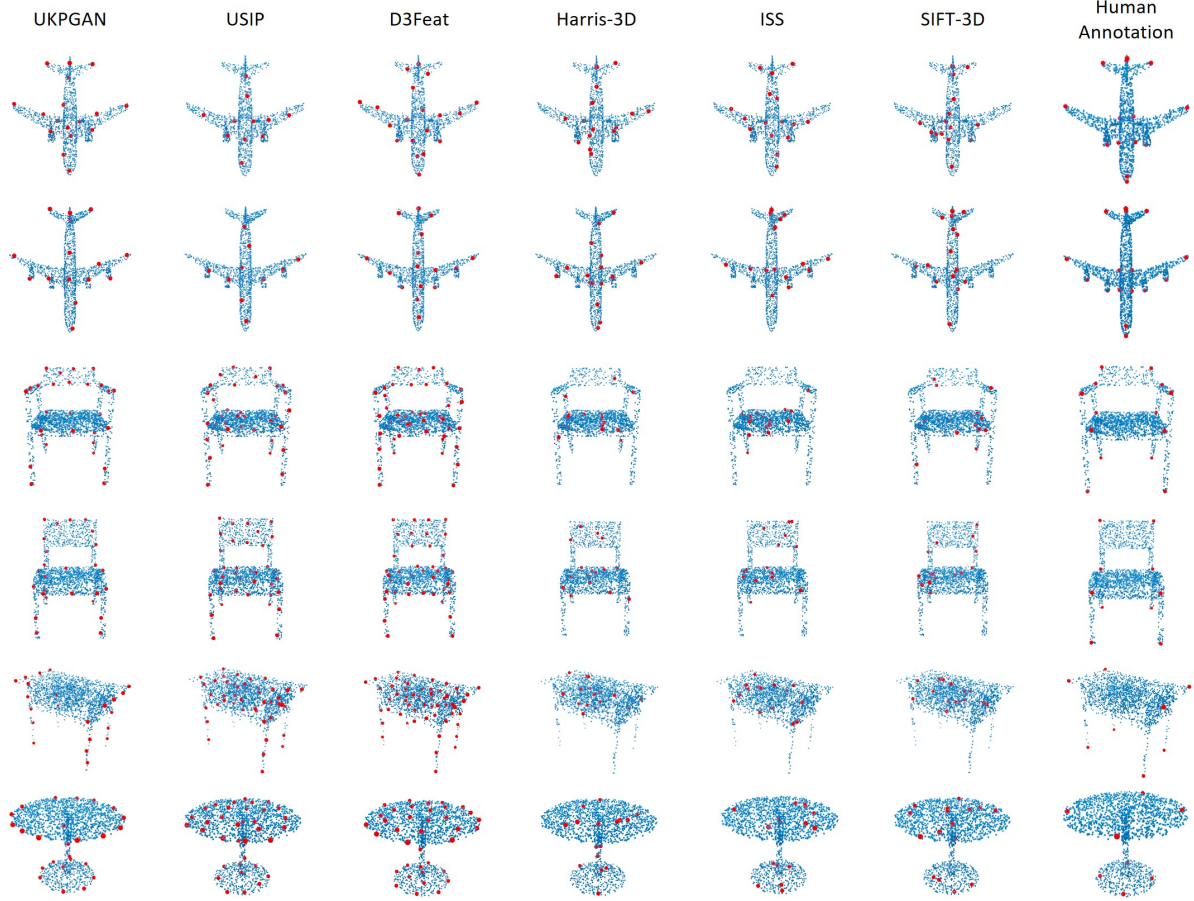


Figure 4: Visualizations of six algorithms on unsupervised keypoint detection on ShapeNet models.

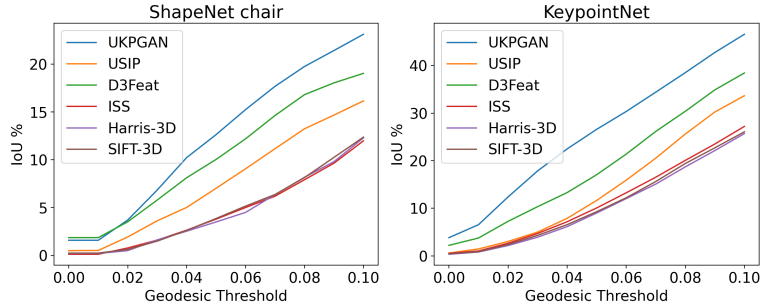


Figure 5: mIoU results on ShapeNet chair dataset and KeypointNet.

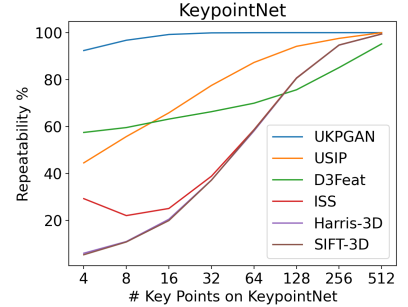


Figure 6: Rotational repeatability.

4.5. Detecting Stable Keypoints with Semantics under Different Human Poses

Dataset Skinned Multi-Person Linear model (SMPL) is a skinned vertex-based model that accurately represents a wide variety of body shapes in natural human poses. Human poses are controlled with three parameters, and we generate training data on the fly by changing these parameters. 2048 points are sampled uniformly from the original mesh.

We take point-wise SHOT descriptors as inputs, which are rotation-invariant and cheap to compute. Point-wise 3D convolution network is replaced with PointNet++ [24] set abstraction layers. For a fair comparison, USIP and D3Feat are evaluated with SHOT as inputs too.

Metric SMPL provides point-to-point correspondence across different human models. Given a pair of models, we

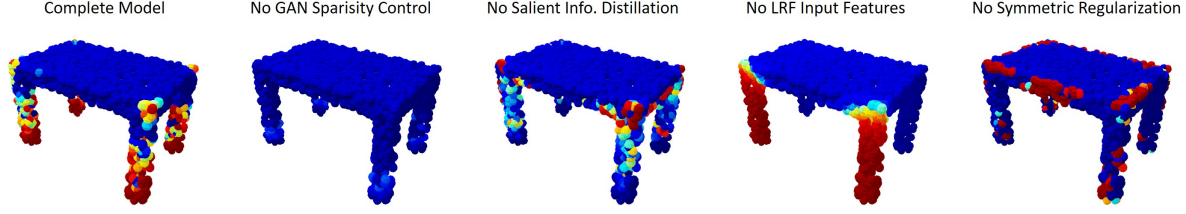


Figure 7: **Visualizations of ablation study on a ShapeNet table.** Colors indicate keypoint probabilities (red means high and blue means low). We see that without GAN sparsity control, our model fails to give meaningful keypoints.

	IoU (%)			Rotation Rep. (%)		
	airplane	chair	table	airplane	chair	table
Ours	68.8	36.2	34.7	98.3	88.3	90.6
Ours w/o GAN Sparsity	36.3	27.2	23.1	99.8	95.9	99.6
Ours w/o Salient Info. Distill.	51.8	33.3	19.0	94.1	87.5	99.9
Ours w/o LRF Feat.	22.4	16.0	21.2	15.4	4.9	0.7
Ours w/o Symmetric Reg.	54.9	20.0	22.3	85.1	77.0	73.0

Table 2: **Results of ablation studies.** Evaluated on ShapeNet models, with KeypointNet test split.

evaluate detectors’ stability and consistency by calculating Intersection of Union (IoU). An intersection is counted if a corresponding point is detected in both models. Union is the sum of all the detected keypoints in both models. Original point clouds are further down-sampled to 1024, 512 points during testing.

Compared Algorithms We evaluate the performance of UKPGAN method and compare it with USIP, D3Feat, Harris-3D, ISS and SIFT-3D. Additionally, we adapt the number of predicted keypoints of baseline methods so that their results are directly comparable to ours.

Evaluation and Results Quantitative results are given in Table 3. Our method achieves the best IoU under different sampling densities, suggesting it is robust and stable.

Qualitative results are shown in Figure 8. We see that UKPGAN is able to generate corresponding stable interest points under different human poses. In addition, it also outputs consist semantic embeddings in an unsupervised way. It is also pretty robust to down-sampling and gives consistent predictions. Notice that our model is trained on models with 2048 points and tested directly on models with 1024 and 512 points, without any fine-tuning.

5. Conclusion

In this work, we proposed an adversarial keypoint detector with adversarial sparsity loss which could detect meaningful points in an unsupervised way. The key contributions of our method are GAN-base sparsity control and salient information distillation modules. Experiments show that

	2048 Points	1024 Points	512 Points
USIP	17.5	14.4	7.8
D3Feat	20.3	18.6	11.2
HARRIS-3D	56.2	47.8	37.8
ISS	36.8	31.1	23.0
SIFT-3D	75.3	64.3	52.9
Ours	91.8	90.6	84.8

Table 3: **IoU (%) of detected keypoints for SMPL dataset, for different downsample ratios.** Our keypoint detector is more stable under different deformations.

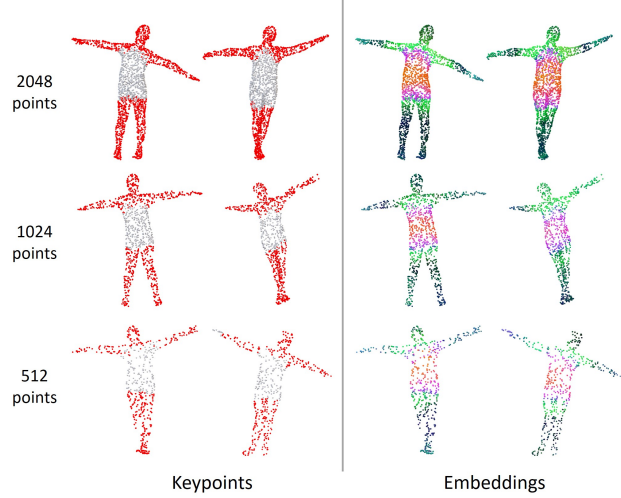


Figure 8: **Keypoint and embedding predictions of our model on SMPL dataset.** Left are keypoint predictions and right are embeddings predictions, best viewed in color. Both keypoint and embedding predictions are consistent across instances, under different downsampling ratios.

our UKPGAN detector can produce more stable keypoints than previous methods in preserving intra-class consistency. Moreover, our method also guarantees the rotation invariance both theoretically and empirically. UKPGAN achieves nearly 100% rotation repeatability even when few points are detected. Last but not least, our UKPGAN detector gives stable and consistent keypoints on non-rigid meshes.

References

- [1] Martin Arjovsky, Soumith Chintala, and Léon Bottou. Wasserstein gan. *arXiv preprint arXiv:1701.07875*, 2017. [3](#)
- [2] Xuyang Bai, Zixin Luo, Lei Zhou, Hongbo Fu, Long Quan, and Chiew-Lan Tai. D3feat: Joint learning of dense detection and description of 3d local features. *arXiv preprint arXiv:2003.03164*, 2020. [1](#), [2](#), [5](#)
- [3] Herbert Bay, Tinne Tuytelaars, and Luc Van Gool. Surf: Speeded up robust features. In *European conference on computer vision*, pages 404–417. Springer, 2006. [2](#)
- [4] M Bueno, J Martínez-Sánchez, H González-Jorge, and H Lorenzo. Detection of geometric keypoints and its application to point cloud coarse registration. *International Archives of the Photogrammetry, Remote Sensing & Spatial Information Sciences*, 41, 2016. [1](#)
- [5] Umberto Castellani, Marco Cristani, Simone Fantoni, and Vittorio Murino. Sparse points matching by combining 3d mesh saliency with statistical descriptors. In *Computer Graphics Forum*, volume 27, pages 643–652. Wiley Online Library, 2008. [1](#), [2](#)
- [6] Angela Dai, Angel X Chang, Manolis Savva, Maciej Halber, Thomas Funkhouser, and Matthias Nießner. Scannet: Richly-annotated 3d reconstructions of indoor scenes. In *Proceedings of the IEEE Conference on Computer Vision and Pattern Recognition*, pages 5828–5839, 2017. [1](#)
- [7] Clara Fernandez-Labrador, Ajad Chhatkuli, Danda Pani Paudel, Jose J Guerrero, Cédric Demonceaux, and Luc Van Gool. Unsupervised learning of category-specific symmetric 3d keypoints from point sets. *arXiv preprint arXiv:2003.07619*, 2020. [2](#)
- [8] Georgios Georgakis, Srikrishna Karanam, Ziyang Wu, Jan Ernst, and Jana Košecká. End-to-end learning of keypoint detector and descriptor for pose invariant 3d matching. In *Proceedings of the IEEE Conference on Computer Vision and Pattern Recognition*, pages 1965–1973, 2018. [2](#)
- [9] Zan Gojcic, Caifa Zhou, Jan D Wegner, and Andreas Wieser. The perfect match: 3d point cloud matching with smoothed densities. In *Proceedings of the IEEE Conference on Computer Vision and Pattern Recognition*, pages 5545–5554, 2019. [3](#)
- [10] Ian Goodfellow, Jean Pouget-Abadie, Mehdi Mirza, Bing Xu, David Warde-Farley, Sherjil Ozair, Aaron Courville, and Yoshua Bengio. Generative adversarial nets. In *Advances in neural information processing systems*, pages 2672–2680, 2014. [3](#)
- [11] Christopher G Harris, Mike Stephens, et al. A combined corner and edge detector. In *Alvey vision conference*, volume 15, pages 10–5244. Citeseer, 1988. [1](#)
- [12] Tong He, Haibin Huang, Li Yi, Yuqian Zhou, Chihao Wu, Jue Wang, and Stefano Soatto. Geonet: Deep geodesic networks for point cloud analysis. In *Proceedings of the IEEE Conference on Computer Vision and Pattern Recognition*, pages 6888–6897, 2019. [1](#)
- [13] Tomas Jakab, Ankush Gupta, Hakan Bilen, and Andrea Vedaldi. Unsupervised learning of object landmarks through conditional image generation. In *Advances in neural information processing systems*, pages 4016–4027, 2018. [2](#)
- [14] Marc Khoury, Qian-Yi Zhou, and Vladlen Koltun. Learning compact geometric features. In *Proceedings of the IEEE International Conference on Computer Vision*, pages 153–161, 2017. [2](#)
- [15] Diederik P Kingma and Max Welling. Auto-encoding variational bayes. *arXiv preprint arXiv:1312.6114*, 2013. [4](#)
- [16] Chang Ha Lee, Amitabh Varshney, and David W Jacobs. Mesh saliency. *ACM transactions on graphics (TOG)*, 24(3):659–666, 2005. [1](#), [2](#)
- [17] Jiaxin Li, Ben M Chen, and Gim Hee Lee. So-net: Self-organizing network for point cloud analysis. In *Proceedings of the IEEE conference on computer vision and pattern recognition*, pages 9397–9406, 2018. [1](#)
- [18] Jiaxin Li and Gim Hee Lee. Usip: Unsupervised stable interest point detection from 3d point clouds. In *Proceedings of the IEEE International Conference on Computer Vision*, pages 361–370, 2019. [1](#), [2](#), [5](#)
- [19] Matthew Loper, Naureen Mahmood, Javier Romero, Gerard Pons-Moll, and Michael J. Black. SMPL: A skinned multi-person linear model. *ACM Trans. Graphics (Proc. SIGGRAPH Asia)*, 34(6):248:1–248:16, Oct. 2015. [4](#)
- [20] David G Lowe. Distinctive image features from scale-invariant keypoints. *International journal of computer vision*, 60(2):91–110, 2004. [1](#), [2](#), [5](#)
- [21] Ajmal S Mian, Mohammed Bennamoun, and Robyn Owens. Three-dimensional model-based object recognition and segmentation in cluttered scenes. *IEEE transactions on pattern analysis and machine intelligence*, 28(10):1584–1601, 2006. [1](#)
- [22] Zak Murez, Tarrence van As, James Bartolozzi, Ayan Sinha, Vijay Badrinarayanan, and Andrew Rabinovich. Atlas: End-to-end 3d scene reconstruction from posed images. *arXiv preprint arXiv:2003.10432*, 2020. [1](#)
- [23] John Novatnack and Ko Nishino. Scale-dependent 3d geometric features. In *2007 IEEE 11th International Conference on Computer Vision*, pages 1–8. IEEE, 2007. [1](#)
- [24] Charles Ruizhongtai Qi, Li Yi, Hao Su, and Leonidas J Guibas. Pointnet++: Deep hierarchical feature learning on point sets in a metric space. In *Advances in neural information processing systems*, pages 5099–5108, 2017. [7](#)
- [25] Ethan Rublee, Vincent Rabaud, Kurt Konolige, and Gary Bradski. Orb: An efficient alternative to sift or surf. In *2011 International conference on computer vision*, pages 2564–2571. Ieee, 2011. [1](#), [2](#)
- [26] Ivan Sipiran and Benjamin Bustos. Harris 3d: a robust extension of the harris operator for interest point detection on 3d meshes. *The Visual Computer*, 27(11):963, 2011. [1](#), [2](#), [5](#)
- [27] Jian Sun, Maks Ovsjanikov, and Leonidas Guibas. A concise and provably informative multi-scale signature based on heat diffusion. In *Computer graphics forum*, volume 28, pages 1383–1392. Wiley Online Library, 2009. [1](#), [2](#)
- [28] Minhuk Sung, Hao Su, Ronald Yu, and Leonidas J Guibas. Deep functional dictionaries: Learning consistent semantic structures on 3d models from functions. In *Advances in Neural Information Processing Systems*, pages 485–495, 2018. [2](#)

- [29] Supasorn Suwajanakorn, Noah Snavely, Jonathan J Tompson, and Mohammad Norouzi. Discovery of latent 3d keypoints via end-to-end geometric reasoning. In *Advances in neural information processing systems*, pages 2059–2070, 2018. 2
- [30] Lyne P Tchapmi, Vineet Kosaraju, Hamid Rezatofighi, Ian Reid, and Silvio Savarese. Topnet: Structural point cloud decoder. In *Proceedings of the IEEE Conference on Computer Vision and Pattern Recognition*, pages 383–392, 2019. 4
- [31] Hanyu Wang, Jianwei Guo, Dong-Ming Yan, Weize Quan, and Xiaopeng Zhang. Learning 3d keypoint descriptors for non-rigid shape matching. In *Proceedings of the European Conference on Computer Vision (ECCV)*, pages 3–19, 2018. 1
- [32] J Gerard Wolff. Information compression as a unifying principle in human learning, perception, and cognition. *Complexity*, 2019, 2019. 2
- [33] Li Yi, Vladimir G. Kim, Duygu Ceylan, I-Chao Shen, Mengyan Yan, Hao Su, Cewu Lu, Qixing Huang, Alla Sheffer, and Leonidas Guibas. A scalable active framework for region annotation in 3d shape collections. *SIGGRAPH Asia*, 2016. 5
- [34] Li Yi, Hao Su, Xingwen Guo, and Leonidas J Guibas. Sync-specnn: Synchronized spectral cnn for 3d shape segmentation. In *Proceedings of the IEEE Conference on Computer Vision and Pattern Recognition*, pages 2282–2290, 2017. 2, 5
- [35] Yang You, Yujing Lou, Chengkun Li, Zhoujun Cheng, Liangwei Li, Lizhuang Ma, Cewu Lu, and Weiming Wang. Keypointnet: A large-scale 3d keypoint dataset aggregated from numerous human annotations. *arXiv preprint arXiv:2002.12687*, 2020. 5
- [36] Yuting Zhang, Yijie Guo, Yixin Jin, Yijun Luo, Zhiyuan He, and Honglak Lee. Unsupervised discovery of object landmarks as structural representations. In *Proceedings of the IEEE Conference on Computer Vision and Pattern Recognition*, pages 2694–2703, 2018. 2
- [37] Yu Zhong. Intrinsic shape signatures: A shape descriptor for 3d object recognition. In *2009 IEEE 12th International Conference on Computer Vision Workshops, ICCV Workshops*, pages 689–696. IEEE, 2009. 1, 2, 5

Supplementary

1. More Results on ShapeNet Part Models

Table 4 gives results of more categories on ShapeNet part dataset, evaluated under mean correspondence ratio (%). Experiment settings are identical to that in Section 4.1. We see that our model achieves the highest average mean correspondence. Some qualitative results are demonstrated in Figure 9.

	Bag	Cap	Car	Earphone	Guitar	Knife	Lamp	Laptop	Motorbike	Mug	Pistol	Rocket	Skateboard	Average
USIP	83.4	81.8	71.8	82.2	92.3	86.8	61.6	91.6	70.6	94.4	81.1	83.1	75.6	81.3
D3Feat	84.9	80.9	76.7	78.9	92.1	90.0	59.6	92.2	73.0	92.8	88.0	79.6	81.8	82.3
HARRIS-3D	91.7	81.5	73.9	86.1	90.6	87.3	68.1	86.8	68.0	95.0	90.3	80.5	83.7	83.3
ISS	95.8	81.9	73.1	80.1	88.0	88.8	65.1	89.3	75.9	96.4	91.1	80.1	79.9	83.5
SIFT-3D	88.9	78.3	71.5	77.4	89.4	88.0	67.5	85.4	71.9	94.6	93.3	83.1	83.7	82.5
Ours	89.2	76.0	78.9	82.3	90.7	90.4	64.0	99.3	85.7	99.5	88.6	74.5	72.3	84.0

Table 4: **Mean correspondence ratio (%) evaluated on ShapeNet part dataset.** Our method gives the highest correspondence ratio compared with human annotations.

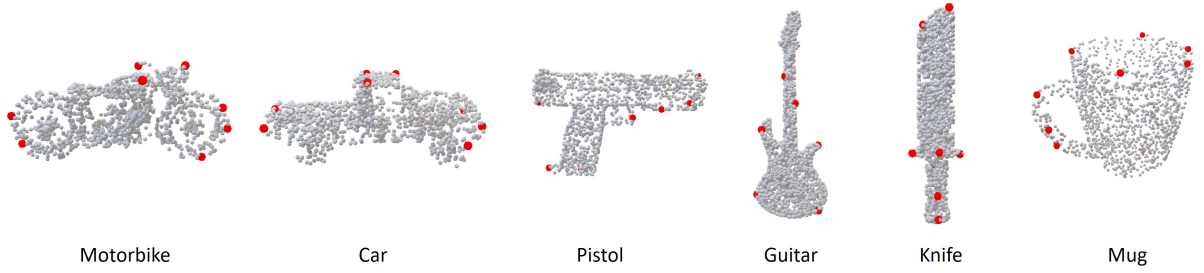


Figure 9: **Some qualitative visualizations of our keypoint detector on ShapeNet models.**

2. More Analysis on Keypoint Controllability with Beta Distribution

In Beta distributions, we have α and β controlling the keypoint probability accumulation around 0 and 1, respectively. This controllability is illustrated in Figure 10. We see that our model automatically identify those semantic keypoints with certain distribution requirements.

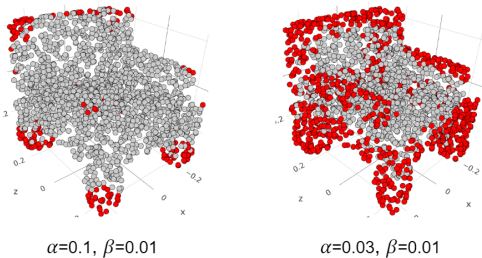


Figure 10: We can easily control the number of keypoints with Beta distribution parameters. Keypoints are shown in red with $p > 0.5$.

3. Extension on Unsupervised 2D Binary Image Analysis

Our method is not only restricted to 3D shape analysis but 2D binary images. In this experiment, we evaluate our method on MNIST, by viewing each pixel as a 2D point. The encoder is replaced with 2D convolution without local reference frame. Digits from all classes are trained jointly.

The results on unsupervised keypoint detection is shown in Figure 11. It can be shown that our algorithm captures important keypoint skeletons in MNIST digits and they are consistent within each class. In the meantime, unsupervised dense embeddings are also predicted for each pixel. Quite interestingly, the generated embeddings (Figure 12) are consistent within each class, without acquiring any class label at training time.

4. More Visualizations on Detected Keypoints under Arbitrary Rotations

We plot more visualization results in Figure 13, where each model is rotated four times. We see that UKPGAN does a pretty good job in maintaining rotation repeatability.

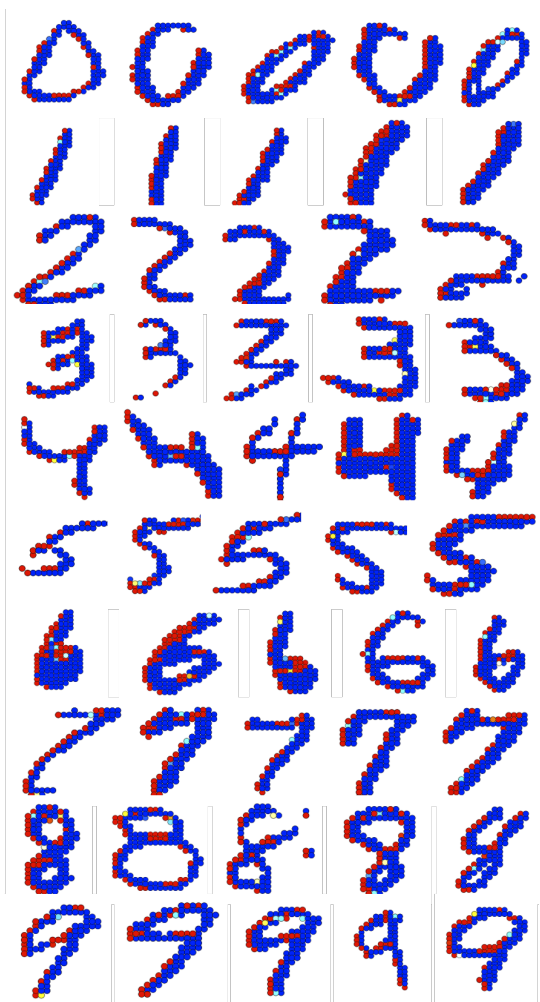


Figure 11: **Keypoint probability heat-map on MNIST.** Red indicates high probability.

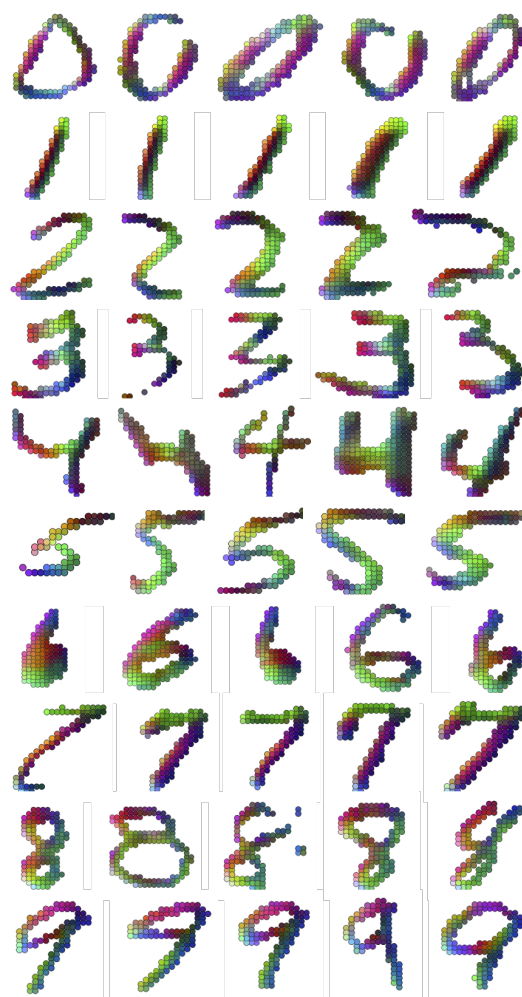


Figure 12: **Dense embeddings generated on MNIST, which are consistent across digits within the same class.** Best viewed in color.

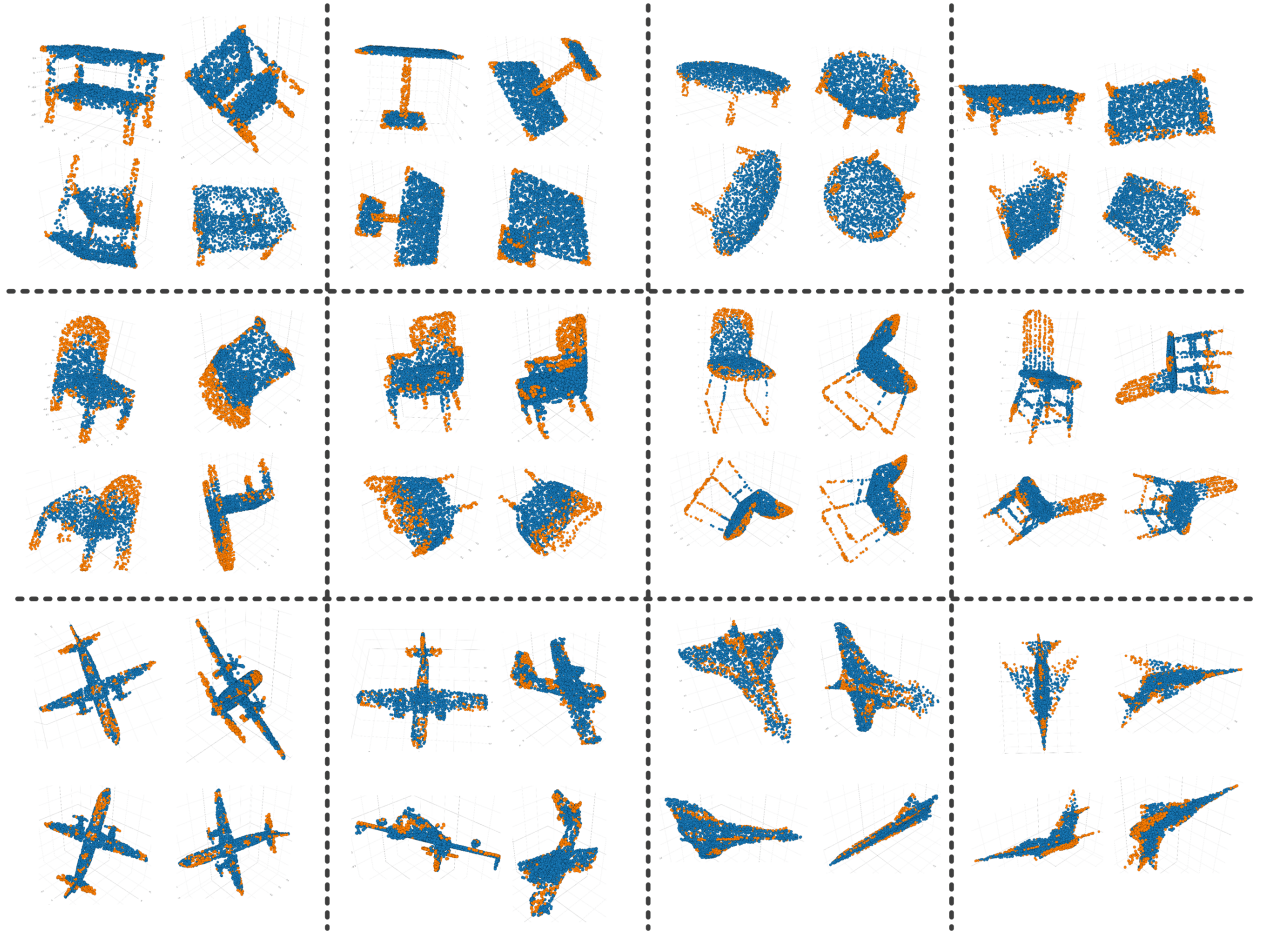


Figure 13: More visualization results. Each model is rotated four times. Point clouds are shown in blue while keypoints are shown in orange.